Surface Chemistry

DOI: 10.1002/anie.201202598

Reversible Wurtzite–Tetragonal Reconstruction in ZnO(10$\bar{1}$0) Surfaces**

*Mo-Rigen He, Rong Yu, and Jing Zhu**

As an important functional material, ZnO is extensively applied in ultraviolet optoelectronics,[1] piezoelectric energy harvesting,[2] gas sensors,[3] and heterogeneous catalysts,[4] and its crystal structure and phase stability play dominant roles in the performances of these devices.[5] Hence the rich polymorphism of ZnO has been noticed for several decades. Besides the commonly observed wurtzite (WZ) structure, rocksalt,[6] zinc-blende,[7] graphite-like hexagonal,[8] and body-centered-tetragonal (BCT) structures[9,10] have been reported till now, mainly based on in situ X-ray diffraction and atomistic simulations. However, these stress-induced new polymorphs, and especially their transition processes, have been seldom observed directly at atomic scale.

Exposure of surfaces can also lead to phase transition, as widely revealed in covalent,[11] metallic,[12,13] and oxide surfaces.[14] Modifications of surface structures may also open new prospects for the applications based on ZnO nanomaterials,[1–4] however, the surface reconstruction in ZnO(10$\bar{1}$0), one of the most basic surfaces in ionic crystals, was still far from well understood. Although a WZ-BCT reconstruction (see Figure 1) was frequently predicted for the similar GaN(10$\bar{1}$0) and AlN(10$\bar{1}$0) surfaces by atomistic simulations,[15,16] this kind of surface phase transition has never been verified in experiments, because the unchanged (1 × 1) surface symmetry makes it difficult to be observed using the classic surface-science techniques such as scanning tunneling microscopy (STM),[17] while the profile imaging technique in conventional high-resolution transmission electron microscopy (HRTEM) had suffered from the limited resolution.[18] Thanks to the development of aberration-corrected TEM,[19] it has become feasible to characterize the surface structural behavior directly at atomic scale,[20–23] and most recently, the relaxation of ZnO(10$\bar{1}$0) fresh surfaces was quantified to picometer-level accuracies,[24] thus enabling the identification of any possible phase transitions in surfaces. Herein, we provide the first experimental evidence for the reversible WZ-BCT reconstruction in ZnO(10$\bar{1}$0) surfaces by using aberration-corrected TEM, and energetic calculations based on density functional theory (DFT) are carried out to reveal the transition mechanism.

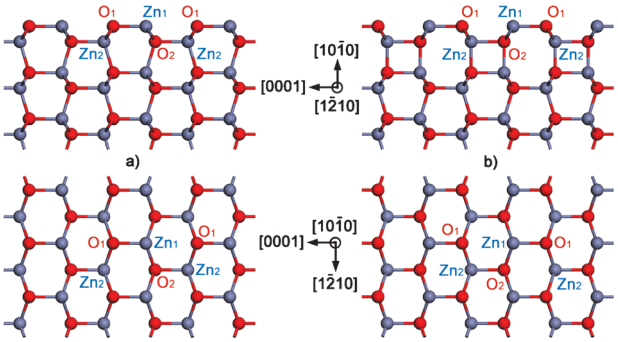

Figure 1. Atomic configurations of the ZnO(10$\bar{1}$0) surface a) before and b) after WZ-BCT reconstruction in the outmost layers. The realistic surface relaxations are not displayed here. WZ and BCT surfaces can be directly distinguished in side-views (top row, in [1$\bar{2}$10] zone axis) as in TEM profile imaging, but are not distinguishable in top-views (bottom row, in [10$\bar{1}$0] zone axis) as in STM. Blue: Zn; red: O.

As described in our previous work,[24] single-crystalline ZnO nanoislands (NIs) were in situ formed inside a TEM (Titan 80-300, FEI) equipped with a spherical aberration (Cs) corrector for the objective lens during intense irradiation with the 300 kV electron beam, and experimental HRTEM images of their at the atomic level clean (10$\bar{1}$0) surfaces were recorded (when the electron beam was spread to larger than full screen) using the negative Cs imaging technique.[25,26] HRTEM image simulations were performed using the multi-slice method as implemented in the MacTempas program,[27] during which the overfocus, specimen thickness, and specimen tilts from the exact [1$\bar{2}$10] zone axis were determined using the maximum cross-correlation method.[24] Equilibrium structures and energetics of the ZnO(10$\bar{1}$0) surface were calculated using the projector augmented-wave method within DFT,[28] as implemented in the VASP program.[29,30] An orthorhombic supercell of 40.0 Å × 5.284 Å × 3.298 Å containing 36 atoms (i.e., 18 layers of (10$\bar{1}$0) plus about 16 Å thick vacuum) was used to model the homogeneously reconstructed surface. More detailed parameters in experiments and calculations can be found in the Supporting Information.

Figure 2a shows the experimental HRTEM image of a ZnO NI with reconstructed (10$\bar{1}$0) surface. As the inner part of the NI remained conventional WZ structure based on six-atom rings, the outmost surface layers manifested a new lattice based on alternating four-atom and eight-atom rings,

[*] Dr. M. He, Prof. R. Yu, Prof. J. Zhu
Beijing National Center for Electron Microscopy
Laboratory of Advanced Materials
Department of Materials Science and Engineering
Tsinghua University, Beijing 100084 (China)
E-mail: jzhu@mail.tsinghua.edu.cn

[**] This work was supported by the National 973 Project of China (grant numbers 2009CB623700 and 2011CB606403), the National Natural Science Foundation of China (grant numbers 50831001 and 51071092), and the Innovation Method Program (grant number 2010IM031300). This work made use of the resources of Beijing National Center for Electron Microscopy.

Supporting information for this article is available on the WWW under http://dx.doi.org/10.1002/anie.201202598.

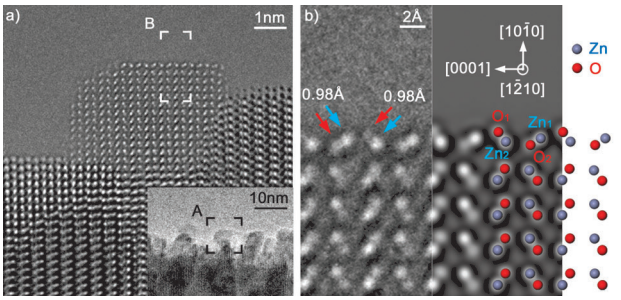

Figure 2. a) Experimental HRTEM image of a ZnO NI with (10$\bar{1}$0) fresh surface reconstructed from WZ to BCT lattice (viewed along [1$\bar{2}$10] zone axis). No filtering was applied. Inset: low-magnification TEM image of the side surface of a nanowire on which the ZnO NIs were grown. The frame A corresponds to (a). b) Left column: enlarged view of the frame B in (a). Right column: simulated HRTEM image (with overfocus of 5.6 nm, specimen thickness of 4.2 nm, and specimen tilt of 7 mrad toward [0001] direction) and atomic configuration of the reconstructed ZnO(10$\bar{1}$0) surface.

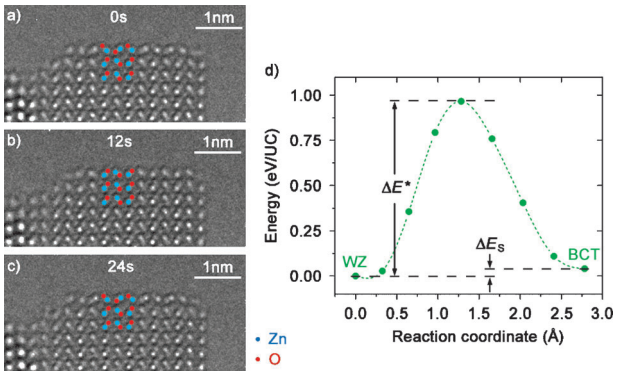

Figure 3. a–c) A series of experimental HRTEM images showing the back-and-forth reconstructions of a NI surface: a) BCT, b) WZ, and c) BCT. d) DFT-calculated MEP of WZ-BCT reconstruction in the ZnO-(10$\bar{1}$0) free surface.

which is characteristic of the BCT structure in Figure 1b. Figure 2b shows the atomic configuration and simulated HRTEM image of the reconstructed ZnO(10$\bar{1}$0) surface. Qualitatively, one-to-one correspondence was noted between the intensity peaks in experimental image and the simulated positions of atomic columns. Moreover, the nearest-neighboring Zn and O atoms on the surface were directly resolved, and their interatomic projective distances were measured to be (0.981 ± 0.069) Å for Zn_1-O_2 and (0.976 ± 0.071) Å for O_1-Zn_2, agreeing quantitatively well with the 0.985 Å for Zn_1-O_2 and 0.978 Å for O_1-Zn_2 in DFT calculations. Also, these distances were smaller than the value of 1.14 Å in bulk ZnO, manifesting the relaxations in realistic BCT surface, that is, the inward displacement of Zn_1 and outward displacement of Zn_2, as similarly observed in the relaxed WZ surface.[24] Thereby, it is unambiguously confirmed that the outmost atomic layers of the ZnO(10$\bar{1}$0) surface, as predicted in previous atomistic simulations,[15,16] can be reconstructed from the WZ to BCT lattice.

Importantly, we noted that the BCT surface was only observed for a part of the NIs (16 out of 54 observations), while the other NIs in our experiments still manifested the WZ surface (see in the Supporting Information section S1). But once transformed, interestingly, while most of the BCT surfaces remained stable during the observations, the inverse reconstruction from the BCT to the WZ surface or back-and-forth reconstructions were still occasionally observed (5 out of 16 observations), as typically shown in Figure 3a,b, and c. To understand the mechanism of such reversible surface reconstruction, the transition energetics were calculated using the nudged elastic band (NEB) method,[31] and the minimum energy path (MEP) of reconstruction in ZnO(10$\bar{1}$0) free surface was shown in Figure 3d. For each unit cell (UC, containing two Zn–O pairs) on the surface, the transition barrier (ΔE^*) of 0.966 eV per UC was much lower than the energy (E_{TF}) that can be transferred from the 300 kV electron beam to the nuclei, the maximum value of which was about 13.3 eV for the Zn atom and 53.2 eV for the O atom.[32] Therefore in principle, the surface reconstruction can be activated by the electron-beam irradiation. On the other hand, the energy of the BCT surface was higher than that of the WZ surface by only 0.040 eV per UC (ΔE_S), which was much smaller than the ΔE^*. As a result, ΔE^* was nearly identical to $\Delta E^* - \Delta E_S$, and thus, the ZnO(10$\bar{1}$0) surface was in an intrinsically bistable state so that the transformation propensity for the WZ surface was quite close to that for the BCT surface, which is in agreement with our experimental observations that the "transformation rate" from the WZ to the BCT surface ($16/54 = 0.296$) was similar to that from the BCT to the WZ surface ($5/16 = 0.313$).

Practically, the kinetic stability of surfaces under electron-beam irradiation was also dependent on the cross-section of the scattering event that can provide sufficient E_{TF} to overcome the total transition barrier, which scaled with the area of reconstructed surface (see the Supporting Information for details). For instance, the probability for activating the homogeneous reconstruction of the whole NI surface was only about 0.10 events per minute (from WZ to BCT) and 0.22 events per minute (from BCT to WZ), given the electron-beam intensity of about 50 A cm^{-2} and a typical NI with (10$\bar{1}$0) surface area of (3 nm)^2, which means the initial NI surfaces cannot be reconstructed even within 10 minutes, but this was clearly not the case in our experiments. In comparison, these probabilities can be increased to 4.4 events per minute (from WZ to BCT) and 5.0 events per minute (from BCT to WZ) for a reconstructed area of (2 nm)^2, which accorded better with the coexistence of WZ and BCT surfaces as observed. Thus, the scattering cross-section that drastically decreased with increasing E_{TF} indicated an inhomogeneous mechanism of surface reconstruction, which was also reasonable in view of the localized nature of the electron–nucleus interactions.

Attractively, Figure 4a does show a BCT nucleus, with a width of 2–3 UC, formed on the left edge of a WZ surface, though the nucleus was later on retracted instead of growing further (see in the Supporting Information section S3). Moreover, the (0001) domain boundary between WZ surface and BCT nucleus, with a width of only one Zn–O pair, was directly resolved at atomic scale, and its equilibrium configuration was modeled using DFT calculations. Briefly, the

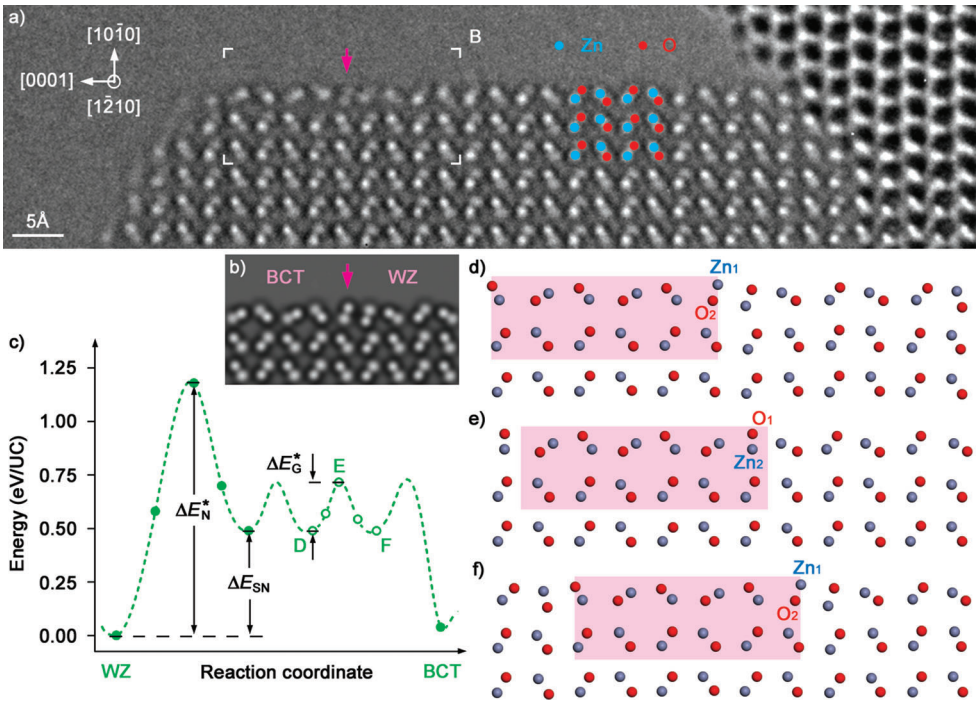

Figure 4. a) Experimental HRTEM image of a ZnO NI with a BCT nucleus emerging from the edge of the WZ surface. The position of domain boundary is indicated by an arrow. b) Simulated HRTEM image (with overfocus of 4 nm, specimen thickness of 4 nm, and no specimen tilts) of the WZ-BCT domain boundary. c) DFT-calculated MEPs for the nucleation (solid circles) and movement (open circles) of a BCT domain in WZ surface. Dash curve shows schematic MEP for the nucleation-growth mechanism (the last energy drop indicates the release of domain boundary energy as the reconstruction is completed). d)–f) Evolution of the atomic configuration in the (10$\bar{1}$0) surface during the movement of the BCT domain (shadowed area). Domain boundaries are labeled by the Zn–O pairs undergoing cross-shuffling. Panels (d–f) correspond to D–F in (c), respectively. Blue: Zn; red: O.

above 36-atoms supercell was enlarged in [0001] direction by six times, and a BCT domain with width of 3 UC in [0001] direction was introduced in the first two layers of (10$\bar{1}$0) surface, more details can be found in the Supporting Information. There can be two types of WZ-BCT domain boundaries because of the polarity of the WZ lattice, and Figure 4b shows the simulated HRTEM image corresponding to the case that the BCT domain was at the Zn-terminated side of the WZ domain, which agreed qualitatively well with Figure 4a. The domain boundary was found at a Zn_1–O_2 pair, which was nearly perpendicular to the (10$\bar{1}$0) surface and can be regarded as a transition state between the WZ and BCT configurations. Therefore, we proposed that the domain boundary was possible to migrate through the rotation of the Zn_1–O_2 pair, and thus, the reversible surface reconstruction can be realized by a nucleation-growth approach, which was further shown by our DFT calculations to be energetically more favored than the homogeneous mechanism.

The MEPs for nucleating a BCT domain in the WZ surface and moving it in [0001] direction were calculated using the NEB method, and Figure 4c outlines a schematic MEP of the surface reconstruction following the nucleation-growth mechanism. Since ΔE_N^* of 1.180 eV (per UC in the BCT domain) for the nucleation process was quite close to ΔE^* of 0.966 eV per UC for the homogeneous reconstruction, the total transition barrier can be remarkably lowered because of the decrease of the activated surface area, and thus, the probability for activating a BCT (or WZ) nucleus in a WZ (or BCT) surface can be much higher than that for activating the whole NI surface. Moreover, Figure 4d,e, and f reveal that the movement of the BCT domain can be realized through successive cross-shuffling of the Zn_1–O_2 pair on the domain boundary and its adjacent O_1–Zn_2 pair, and the ΔE_G^* for moving a single domain boundary was only 0.225 eV (per UC on the domain boundary), which was much smaller than the transition barrier (ΔE_N^*–ΔE_{SN} = 0.690 eV per UC) for the recovery of a BCT nucleus to the WZ surface. On the other hand, the ΔE_G^* of about 0.056 eV per atom was quite comparable with $k_B T$ of 0.035 eV per atom (the temperature increase of NIs because of electron–electron interactions was estimated to be about 100 K, see in the Supporting Information section S2 for details). Consequently, as long as a BCT nucleus was activated by the electron beam, its growth process was prone to be driven by the thermal fluctuation (before the next activation event), and thus, the WZ-BCT reconstruction can be spontaneously completed, and vice versa. We should finally state that the nucleus growth in real NIs was also possibly impeded by some (though not well known yet) kinetic factors, which may explain the retraction of the BCT nucleus in Figure 4a, however, it were also these impediments that held the nucleus in a metastable state and enabled us to capture it experimentally.

In summary, the reversible WZ-BCT reconstruction in the outmost layers of ZnO(10$\bar{1}$0) surfaces was activated by electron-beam irradiation and directly revealed with atomic resolution by using aberration-corrected TEM combined with DFT calculations, manifesting the novel intrinsic bistability of ZnO(10$\bar{1}$0) surfaces. Moreover, a nucleation-growth mechanism for surface reconstruction was proposed based on atomic-scale observations and energetic calculations of the (0001) domain boundary between the WZ surface and the BCT nucleus. Our studies provided more comprehensive insight into the surface structure and its dynamic behavior of the widely used and important class of crystals with WZ lattice, and aberration-corrected TEM was shown to be promising for exploring the metastable atomic configurations of surfaces as well as nanomaterials.[23] Hopefully, more light

can be shed on the dynamic transition processes given the persistent improvements in spatial and temporal resolutions, and the effects of surface reconstruction on the physical and chemical properties of materials (such as piezoelectricity and surface electronic states) can be an intriguing issue for future research.

Received: April 3, 2012
Revised: May 21, 2012
Published online: June 22, 2012

Keywords: ab initio calculations · electron microscopy · metal oxides · phase transitions · surface chemistry

[1] Ü. Özgür, Ya. I. Alivov, C. Liu, A. Teke, M. A. Reshchikov, S. Doğan, V. Avrutin, S.-J. Cho, H. Morkoç, *J. Appl. Phys.* **2005**, *98*, 041301.
[2] Z. L. Wang, J. H. Song, *Science* **2006**, *312*, 242 – 246.
[3] C. Wöll, *Prog. Surf. Sci.* **2007**, *82*, 55 – 120.
[4] B. Meyer, D. Marx, O. Dulub, U. Diebold, M. Kunat, D. Langenberg, C. Wöll, *Angew. Chem.* **2004**, *116*, 6809 – 6814; *Angew. Chem. Int. Ed.* **2004**, *43*, 6641 – 6645.
[5] A. Ashrafi, C. Jagadish, *J. Appl. Phys.* **2007**, *102*, 071101.
[6] C. H. Bates, W. B. White, R. Roy, *Science* **1962**, *137*, 993.
[7] C. Y. Yeh, Z. W. Lu, S. Froyen, A. Zunger, *Phys. Rev. B* **1992**, *46*, 10086 – 10097.
[8] A. J. Kulkarni, M. Zhou, K. Sarasamak, S. Limpijumnong, *Phys. Rev. Lett.* **2006**, *97*, 105502.
[9] J. Wang, A. J. Kulkarni, K. Sarasamak, S. Limpijumnong, F. J. Ke, M. Zhou, *Phys. Rev. B* **2007**, *76*, 172103.
[10] R. Agrawal, B. Peng, H. D. Espinosa, *Nano Lett.* **2009**, *9*, 4177 – 4183.
[11] E. Bengu, R. Plass, L. D. Marks, T. Ichihashi, P. M. Ajayan, S. Iijima, *Phys. Rev. Lett.* **1996**, *77*, 4226 – 4228.
[12] D. S. Su, T. Jacob, T. W. Hansen, D. Wang, R. Schlögl, B. Freitag, S. Kujawa, *Angew. Chem.* **2008**, *120*, 5083 – 5086; *Angew. Chem. Int. Ed.* **2008**, *47*, 5005 – 5008.
[13] X. Huang, H. Li, S. Z. Li, S. X. Wu, F. Boey, J. Ma, H. Zhang, *Angew. Chem.* **2011**, *123*, 12453 – 12456; *Angew. Chem. Int. Ed.* **2011**, *50*, 12245 – 12248.
[14] O. Dulub, U. Diebold, G. Kresse, *Phys. Rev. Lett.* **2003**, *90*, 016102.
[15] P. Xiao, X. Wang, J. Wang, F. J. Ke, M. Zhou, Y. L. Bai, *Appl. Phys. Lett.* **2009**, *95*, 211907.
[16] H. G. Ye, G. D. Chen, Y. L. Wu, Y. Z. Zhu, S. H. Wei, *Phys. Rev. B* **2009**, *80*, 033301.
[17] O. Dulub, L. A. Boatner, U. Diebold, *Surf. Sci.* **2002**, *519*, 201 – 217.
[18] Y. Ding, Z. L. Wang, *Surf. Sci.* **2007**, *601*, 425 – 433.
[19] K. W. Urban, *Science* **2008**, *321*, 506 – 510.
[20] R. Yu, L. H. Hu, Z. Y. Cheng, Y. D. Li, H. Q. Ye, J. Zhu, *Phys. Rev. Lett.* **2010**, *105*, 226101.
[21] L. P. Hansen, Q. M. Ramasse, C. Kisielowski, M. Brorson, E. Johnson, H. Topsøe, S. Helveg, *Angew. Chem.* **2011**, *123*, 10335 – 10338; *Angew. Chem. Int. Ed.* **2011**, *50*, 10153 – 10156.
[22] N. Shibata, A. Goto, S.-Y. Choi, T. Mizoguchi, S. D. Findlay, T. Yamamoto, Y. Ikuhara, *Science* **2008**, *322*, 570 – 573.
[23] H. M. Zheng, J. B. Rivest, T. A. Miller, B. Sadtler, A. Lindenberg, M. F. Toney, L. W. Wang, C. Kisielowski, A. P. Alivisatos, *Science* **2011**, *333*, 206 – 209.
[24] M. He, R. Yu, J. Zhu, *Nano Lett.* **2012**, *12*, 704 – 708.
[25] C. L. Jia, M. Lentzen, K. Urban, *Science* **2003**, *299*, 870 – 873.
[26] K. W. Urban, C. L. Jia, L. Houben, M. Lentzen, S. B. Mi, K. Tillmann, *Philos. Trans. R. Soc. London Ser. A* **2009**, *367*, 3735 – 3753.
[27] J. M. Cowley, *Diffraction Physics*, North-Holland, New York, **1975**.
[28] P. E. Blöchl, *Phys. Rev. B* **1994**, *50*, 17953 – 17979.
[29] G. Kresse, J. Furthmüller, *Comput. Mater. Sci.* **1996**, *6*, 15 – 50.
[30] G. Kresse, J. Furthmüller, *Phys. Rev. B* **1996**, *54*, 11169 – 11186.
[31] G. Henkelman, B. P. Uberuaga, H. Jónsson, *J. Chem. Phys.* **2000**, *113*, 9901 – 9904.
[32] J. H. Zhan, Y. Bando, J. Q. Hu, D. Golberg, *Appl. Phys. Lett.* **2006**, *89*, 243111.

